JOURNAL OF SOLID STATE CHEMISTRY **129,** 130–143 (1997)
ARTICLE NO. SC967251

Structural Characterization of the High-Temperature Phase Transitions in $Ca_8[Al_{12}O_{24}](MoO_4)_2$ Aluminate Sodalite Using X-ray Powder Diffraction

Sander van Smaalen,*,[1] Robert Dinnebier,* Hannelore Katzke,† and Wulf Depmeier†

*Laboratory of Crystallography, University of Bayreuth, Universitätsstrasse 30, D-95440 Bayreuth, Germany; and †Mineralogisches Institut, University of Kiel, Olshausenstrasse 40, D-24098 Kiel, Germany

Received August 5, 1996; in revised form November 25, 1996; accepted November 27, 1996

The structures are reported of the room-temperature and the three high-temperature phases of $Ca_8[Al_{12}O_{24}](MoO_4)_2$ aluminate sodalite CAM. Structure refinements have been performed with the Rietveld method using synchrotron radiation X-ray powder diffraction data. The cubic phase has symmetry $I\bar{4}3m$ with $a = 9.29377(4)$ Å. The tetragonal phases have symmetry $P\bar{4}c2$, and their unit cells corresponds to a $\sqrt{2}a \times \sqrt{2}a \times c$ supercell of the cubic phase. The second tetragonal phase (T2) exists for $614 < T < 624$ K and has lattice parameters $a = 13.14536(6)$ Å and $c = 9.29224(8)$ Å. The first tetragonal (T1) phase is stable for $590 < T < 614$ K and has lattice parameters $a = 13.12263(5)$ Å and $c = 9.32081(5)$ Å, The orthorhombic phase has symmetry $Aba2$ with $a = 26.14683(8)$ Å, $b = 13.07061$ Å, and $c = 9.31413(2)$ Å. The transition (on decreasing temperatures) at $T_c \approx 624$ K, from the cubic to the T2 phase, is of second order and is found to be related to change in the orientational order of the cage anions MoO_4^{2-}. The T2 to T1 transition at $T_c \approx 614$ K is of first order, and it corresponds to a displacement of the cage anions to an off-center position in the cages, while keeping orientational disorder over at least two orientations. The transition at $T_c \approx 590$ K, from the T1 phase to the orthorhombic phase, is again a first-order transition, and it is related to a complete ordering of the cage anions. A detailed description is given of the structural distortions of the framework, accompanying the phase transitions. © 1997 Academic Press

1. INTRODUCTION

The structural family of sodalites belongs to the large class of tetrahedral framework structures. A general, idealized, formula is $M_8[T_{12}O_{24}]X_2$ with M being relatively big cations or anions, and T highly charged small cations (Si, Al, ...). The centers of the corner-sharing TO_4 tetrahedra lie on a three-dimensional net which contains relatively big cages of only one kind. The cages have ideally the shape of a regular truncated octahedron. These highly symmetric polyhedra are connected with each other via common 4-rings and 6-rings in the cubic $\langle 100 \rangle$ and $\langle 111 \rangle$ directions, respectively. The 6-rings are the loci of the M cations, and the X anions are located at the centers of the cages. The cages are commonly called sodalite cages, or β-cages. Although relatively big, the cages are not big enough to allow typical zeolite exchange properties. Despite this fact, the sodalites have often been considered as model cases for zeolites, because of their relatively simple topology, their generally high symmetry, and their quite well-defined chemistry.

Phase transitions may occur connected to structural distortions of the framework (1, 2). Alternatively, for the subfamily of aluminate sodalites with T = Al and with X replaced by XO_4 (X = S, Cr, Mo, W), phase transitions are possible related to rotational order–disorder of the anions. Furthermore, the presence of tetrahedrally shaped oxyanions at the centers of the sodalite cages creates structural peculiarities which are at the origin ferroic properties, modulated and frustrated structures. In the present work we discuss the structures and phase transitions of $Ca_8[Al_{12}O_{24}](MoO_4)_2$, in short notation CAM.

$Ca_8[Al_{12}O_{24}](WO_4)_2$ (CAW) has been studied previously in a series of single-crystal X-ray diffraction experiments. The high-temperature structure ($T > 653$ K) is cubic $I\bar{4}3m$ and exhibits the usual sodalite structure with rotational disorder of the WO_4^{2-} anions (3, 4). At room temperature, the structure is fully ordered on a $2(\mathbf{a} + \mathbf{b})$, $-\mathbf{a} + \mathbf{b}$, $\mathbf{c}$ supercell, with orthorhombic $Aba2$ symmetry (5). An intermediate phase exists which probably has tetragonal symmetry $P\bar{4}c2$ on a $\mathbf{a} + \mathbf{b}$, $-\mathbf{a} + \mathbf{b}$, $\mathbf{c}$ supercell (6).

For CAM, single crystals were not obtained. Using X-ray powder diffraction, indexing of diffraction patterns at various temperatures indicated that CAM should have a cubic phase at temperatures higher than about 643 K, and that it should be orthorhombic at room temperature. Instead of a tetragonal phase as found for CAW, there should be two

[1] To whom correspondence should be addressed.

0022-4596/97 $25.00

intermediate phases for CAM, one of them being tetragonal and the other being incommensurately modulated (7, 8).

In the present paper, we report detailed structures of CAM in its orthorhombic phase, its cubic phase, and the intermediate phases, using synchrotron radiation X-ray powder diffraction, and Rietveld refinements. Two different intermediate phases are identified, both of them with the same tetragonal symmetry.

2. EXPERIMENTAL

The synthesis of CAM was done as described elsewhere (9). Synchrotron radiation X-ray powder diffraction experiments were performed at beam-line X3B1 of the National Synchrotron Light Source at Brookhaven National Laboratory. The diffractometer was equipped with both primary and secondary monochromators, making it possible to record high-resolution, low-background spectra (10). The samples were loaded in capillaries (diameter 0.7 mm) and were rocked during the measurements over a θ range of 20°. The full-width at half-maximum of the reflections at low angles 2θ was 0.010° for the cubic phase, with $\lambda =$ 0.70005 Å. Elevated temperatures were obtained, using a slide-on oven with aluminum foil windows for the radiation (11). The temperature was controlled using a thermocouple element placed near the capillary. The stability of the temperature was about ± 0.5 K; the absolute accuracy is estimated as ± 2 K.

The phase transitions were monitored by measuring the powder diffraction diagrams in a small 2θ range around the cubic $(4, 0, 0)_c$ reflection (12). The amount of splitting of this reflection is an indication of whether the phase is cubic, tetragonal, or orthorhombic. At all temperatures, the resolution of the spectra was sufficient to resolve the different maxima. For structure determination and Rietveld refinement, diffraction patterns were recorded at four different temperatures. The transition between the first tetragonal phase and the orthorhombic phase occurs at approximately 588 K, but with a hysteresis of several kelvin. To obtain a diffractogram of the pure tetragonal phase, the temperature was varied until no contamination could be seen in the diffraction pattern by either orthorhombic or cubic reflections.

The diffraction pattern taken at 298 K could be indexed, starting with the orthorhombic lattice parameters as determined for CAW. A few, spurious, weak diffraction maxima could not be indexed in this way. Probably, they are due to a contamination by one or more phases in the Al–Ca–Mo–O system. An attempt to identify such phases failed. Regions where such reflections occurred as isolated maxima were excluded in the final refinements. A dramatic improvement of the profile R factors was observed on excluding these regions, while atomic coordinates did not depend on whether regions were excluded. Similarly, the experimental diffraction pattern at 648.5 K could be indexed, starting from the cubic lattice constant given for CAW. Indexing the patterns of the tetragonal phases was achieved on a $\sqrt{2}a \times \sqrt{2}a \times a$ supercell of the cubic unit cell.

The first tetragonal phase (T1 phase) measured at $T =$ 604 K, shows spontaneous strain, as is seen by comparing $a_t(T1)/\sqrt{2} = 9.27910$ Å and $c_t(T1) = 9.32081$ Å with $a_c =$ 9.29377 Å. The c lattice parameter is increased and the a and b lattice parameters are decreased in length compared to the cubic lattice constant, while the volumes of the unit cells are the same in both phases (Table 1).

The diffractogram of the second tetragonal phase (T2 phase) at $T = 614$ K could be indexed on a tetragonal lattice, which was obtained as a superlattice of the cubic structure with almost zero strain. This is seen by comparing $a_t(T2)/\sqrt{2} = 9.2952$ Å and $c_t(T2) = 9.2922$ Å with $a_c =$ 9.2938 Å. The experimental parameters are summarized in Table 1.

In addition to the Bragg reflections, the high-temperature patterns showed broad diffuse intensity maxima. We interpret this as diffuse scattering due to the dynamical disorder of the MoO_4^{2-} ions. A background, including this diffuse scattering, was determined by inspection, using the program GUFI (13). The background was subtracted from the experimental intensities, and it was not varied in the Rietveld refinements.

In a second experiment, the temperature dependence between the tetragonal and cubic phases was studied in more detail. First, the splitting of the $(4,0,0)_c$ reflection was studied around $2\theta = 17.327°$ ($\lambda = 0.70005$ Å). In a heating run, an increase of the intensity at the "cubic" position is observed simultaneously with a decrease of the intensities at both "tetragonal" positions at 17.281° and 17.361°, respectively (Fig. 1). Note that the cubic reflection may refer alternatively to $(4,0,0)_c$ of the cubic phase or to both $(0,0,4)_t$ and $(4,4,0)_t$ of the unstrained tetragonal lattice (T2 phase). The reflections at 17.281° and 17.361° are $(0,0,4)_t$ and $(4,4,0)_t$, respectively, of the strained tetragonal lattice (T1 phase). A fit to the observed peaks, with a function, which takes into account the asymmetry of the peaks due to axial divergence (10), resulted in reflection positions which vary less than 0.003° over the whole temperature range. It is clearly determined that it is not the positions, but only the intensities of the three reflections, which vary with temperature. This behavior was found to be reproducible. Below $T = 604$ K, intensity at the cubic position could not be found, while above $T = 611$ K the reflections at the tetragonal positions have disappeared.

Additional information about the behavior of CAM with temperature can be obtained from the temperature dependence of a superlattice reflection, i.e., of a reflection with zero intensity in the cubic phase. To this end, the $(2,1,1)_t$ tetragonal reflection around $2\theta = 8.084°$ was measured as a function of temperature. Profile fits to this isolated peak

TABLE 1
Data Collection Parameters for CAM X-ray Diffraction Experiments at Four Different Temperatures

	Data set			
	Orthorhombic	Tetragonal T1	Tetragonal T2	Cubic
Temperature (K)	298	604	614	648.5
Wavelength (Å)	1.14939	0.70005(3)	0.70005(3)	0.70005(3)
2θ range (°)	4–84	3–63.4	3–52	5–55.2
2θ stepwidth (°)	0.005	0.004	0.004	0.004
Time per step (s)	3	5	5	5
Sample geometry	Flat plate	Capillary	Capillary	Capillary
Space group	*Aba*2	$P\bar{4}c2$	$P\bar{4}c2$	$I\bar{4}3m$
Space group number	41	116	116	217
a (Å)	26.14683 (8)	13.12263 (5)	13.14536 (6)	9.29377 (4)
b (Å)	13.07061 (4)	*a*	*a*	*a*
c (Å)	9.31413 (2)	9.32081 (5)	9.29224 (8)	*a*
Cell volume (Å^3)	4×795.8	2×802.5	2×802.9	802.7
Z	8	4	4	2
R_p	0.099	0.069	0.066	0.084
wR_p	0.138	0.090	0.089	0.116
R_{F^2}	0.069	0.239[a]	0.145	0.101
R_F	0.047	0.242[a]	0.216	0.123
No. of reflections	1411	1584	946	123

[a] The Bragg *R*-factors are high due to the weak scattering above $2\theta = 45°$. For the region 5° to 45°, the values are $R_{F^2} = 0.115$ and $R_F = 0.129$.

showed the reflection position to vary from 8.087° at 594.5 K to 8.082° at 621 K with a scatter of 0.001°. This variation can be explained by normal thermal expansion (expansion coefficient 2.3×10^{-5} K^{-1}). However, it should be noted that the simultaneous decrease of a_t and increase of c_t is compensated to a large extent for this reflection, and that the scattering angle of the $(2, 1, 1)_t$ reflection is independent of the spontaneous strain. The intensity of this reflection varied between its maximum value, attained in the tetragonal phase below $T = 598$ K, and zero in the cubic phase above $T = 624$ K. Noteworthy is that the square of the intensity varies linearly with temperature, with a crossover between two different temperature coefficients at about 608 K (Fig. 2). This behavior was reproducible and hysteresis could not be detected. We conclude from these results that below $T \approx 600$ K, the sample is in its tetragonal T1 phase and that above $T = 624$ K, the sample is cubic. The behavior between $T \approx 600$ K and 624 K will be discussed in Section 4.3.

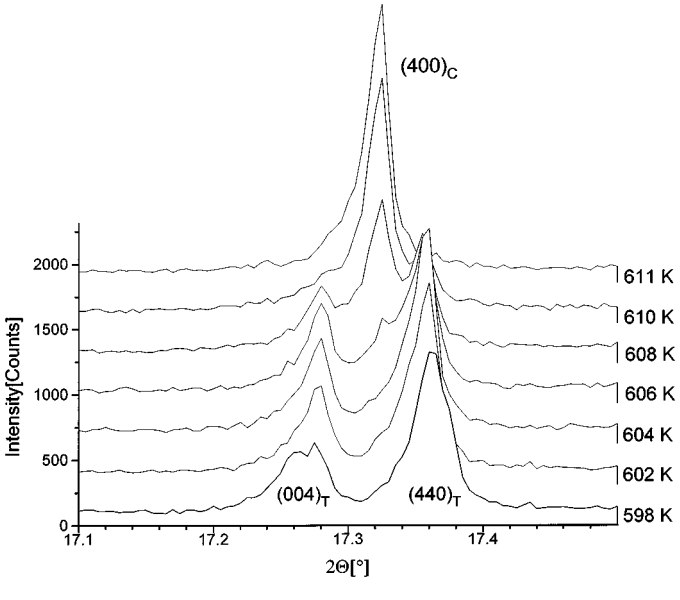

FIG. 1. The diffraction around the $(4, 0, 0)_c$ reflection at various temperatures.

3. STRUCTURE REFINEMENTS

Rietveld refinements were performed with the program GSAS (14). Starting points for the orthorhombic and cubic phases were the coordinates as reported for CAW (4, 5), while replacing W by Mo. A smooth convergence was obtained to the final parameters, and CAM was found to be isostructural to CAW in these phases. Coordinates for the tetragonal T1 phase were obtained by interpolation between those for the orthorhombic and cubic phases. The multiple positions for the oxygen atoms of the disordered MoO_4^{2-} tetrahedra were obtained from a difference Fourier

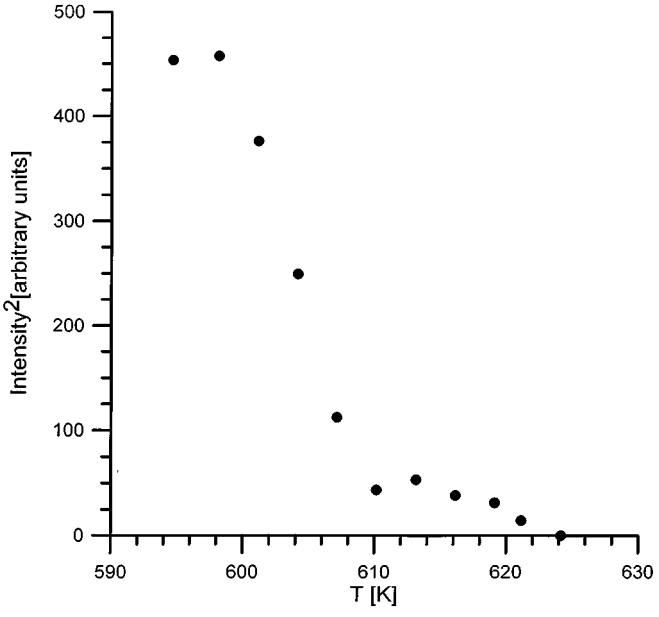

FIG. 2. The intensity of the $(2, 1, 1)_t$ tetragonal reflection at $2\theta = 8.084°$, as a function of the temperature.

map. Starting point for the refinement of the structure of the second tetragonal T2 phase at $T = 614$ K were the coordinates of the T1 phase.

In the initial stages, the profiles were fitted with a pseudo-Voigt function, and the best fit was obtained for an almost pure Lorentzian shape. Due to their high asymmetry, this description of the diffraction peaks is not a good one, and a characteristic plus/minus difference is obtained between observed and calculated intensities (Fig. 3), while the integrated intensities do match. The final refinements were performed with a newly implemented profile function for synchrotron data (14–16), which gave a much better description of the peak shapes. Generally, the effect of this new profile function was an improvement of the fit to the diffraction peaks (Fig. 3) and a lowering of R_p and wR_p by 0.01 or 0.02, while the coordinates did not change more than their standard deviations. Changes of the temperature parameters were on the order of their standard deviations. The standard deviations of coordinates and temperature parameters became about 20% smaller, thus illustrating the better fit. The lattice constants did change by up to 10 times their (very small) standard deviations, and it must be concluded that the effect of the wrong profile function is that of introducing a systematic error, albeit of small size.

Observed and calculated diffraction diagrams for all four measurements are given in Figs. 4 through 7. Coordinates of the atoms of the four phases are given in the Tables 2, 3, 4, and 5. They correspond to the refinements with the new, better peak-shape functions.

4. DISCUSSION

4.1. The Structure of the Framework

The framework of sodalite compounds can be described as built of corner-sharing TO_4 tetrahedra (T = Si, Al, …). Taylor (1) has shown that the thermal expansion of sodalite compounds can be described by a single parameter (the tilt angle ϕ) defining the rotation of these tetrahedra. The fully expanded state has $\phi = 0°$, and corresponds to a symmetry $Im\bar{3}m$. $\phi \neq 0°$ reduces the space group to $I\bar{4}3m$. On increasing ϕ, the specific volume decreases, and a maximum value for ϕ exists, as determined by the sizes of the cavity ions.

It was shown previously that variations in the framework structure can also involve distortions of the tetrahedra, as was observed especially in the case of aluminate sodalites (17). Within cubic symmetry, the tetrahedra can distort such that two opposite angles (α) become larger than 109°, and four angles (α') become smaller. A relation was given between the tetrahedra bond length (d_t), the two angles α and α', the angle ϕ, and the lattice constant (17). Alternatively, the rotation of the tetrahedra can be calculated from the coordinates of the oxygen atom.

The cubic phase of CAM can be described by the degrees of freedom given above, and we find $\alpha = 120.1°$ and $\alpha' = 104.5°$ (Table 6), leading to $\phi = 13.0°$. These values are within the range of other aluminate sodalites, like CAW, SAW, and SAM.

Symmetry lower than cubic allows further distortions of the tetrahedra. Assuming the structure of a free AlO_4 ion to be that of the ideal tetrahedron, distortions then are an indication for a relative instability of the framework. The stability of the compound has other important contributions from the cation-framework, anion-framework, and cation–anion interactions, as well as from entropy effects. The cubic phase is built of one type of distorted tetrahedron (Table 6). The distortion found corresponds to a collapsed state of the framework, determined by the size of the cation and by the cation-framework interaction. Entropic stabilization of the cubic phase will have contributions from the disorder of the anion.

For the fully ordered orthorhombic phase, all seven crystallographically independent AlO_4 tetrahedra have a structure resembling that in the cubic phase: the average bond length within one tetrahedron ranges from 1.72 to 1.78 Å. and there are always two angles of about 120° and four angles in the range 100° to 110° (Table 9). It follows that the structures of the frameworks of the orthorhombic and cubic phases will be of comparable stability. Further contributions to the stabilization of the orthorhombic phase come from the bonding interactions between the framework and both the anions and the ordered cations. The entropic stabilization of the cubic phase due to disorder of the anions is replaced by anion-framework bonding in the orthorhombic phase.

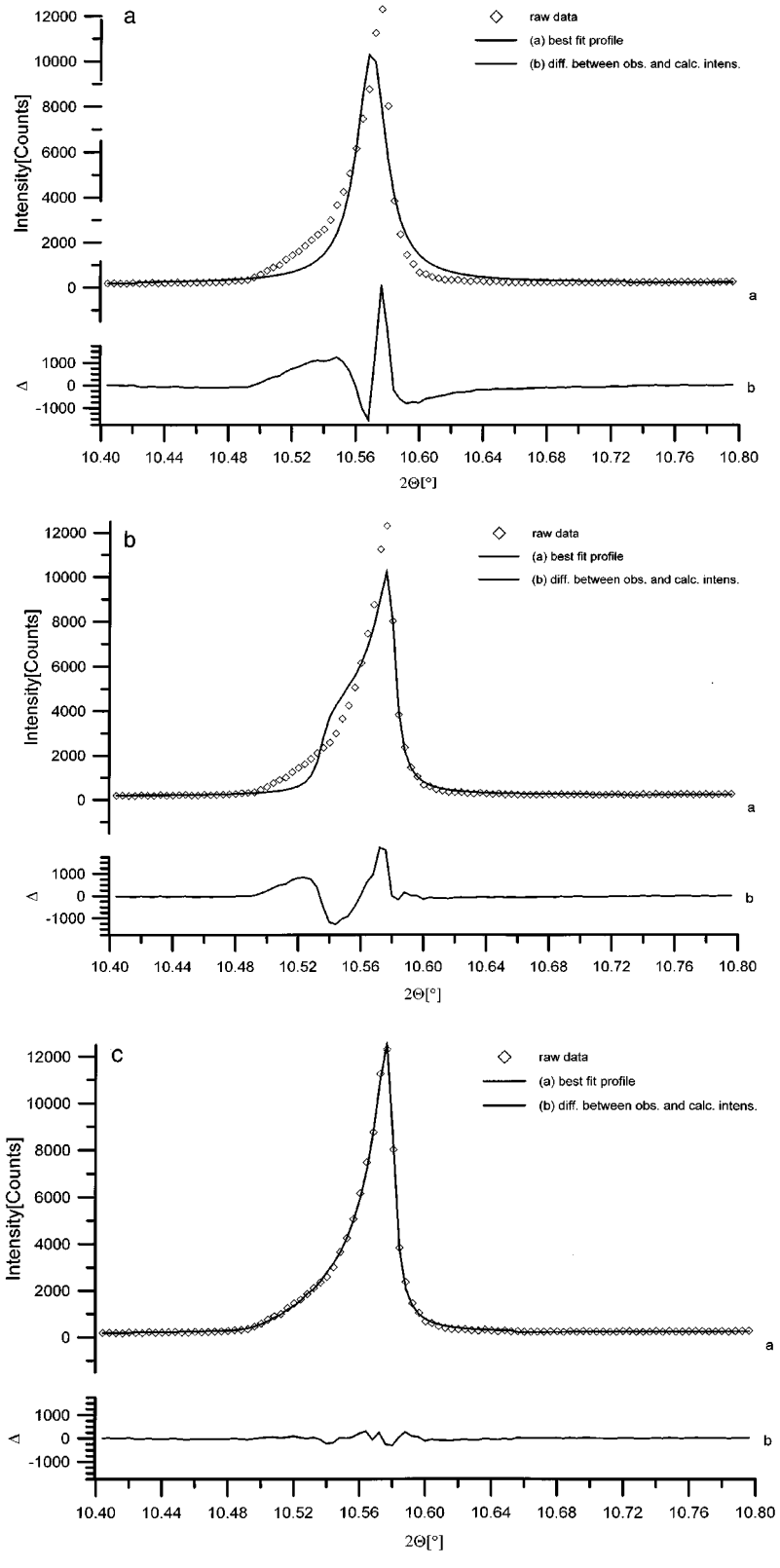

FIG. 3. Experimental data and the fit through X-ray powder diffraction spectra of cubic CAM around the $(2, 1, 1)_o$ reflection, taken from Rietveld refinement of the complete pattern. (a) With the pure pseudo-Voigt function for the profile, leading to $R_p = 0.114$ for the complete pattern. (b) With old asymmetry correction as was implemented in GSAS, leading to $R_p = 0.097$. (c) With the new, synchrotron-adapted profile function for the asymmetry correction in GSAS, used in the final refinements in the present work ($R_p = 0.084$, see Table 1).

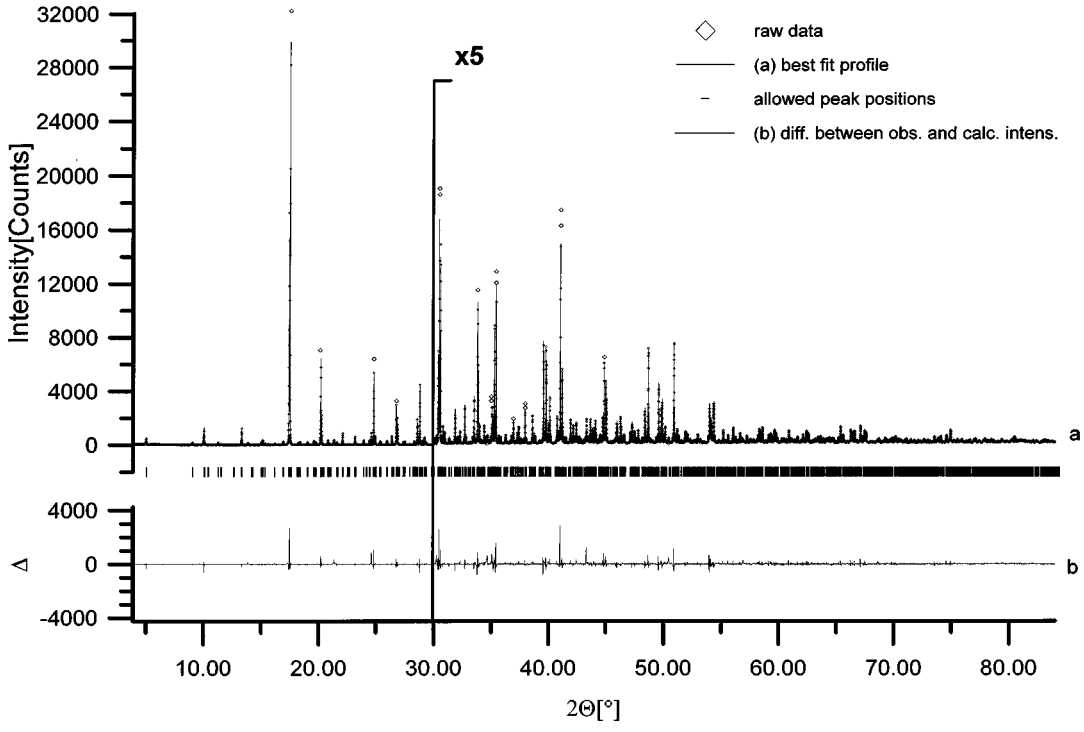

FIG. 4. The X-ray powder diffraction spectra of CAM in its orthorhombic phase at 298 K.

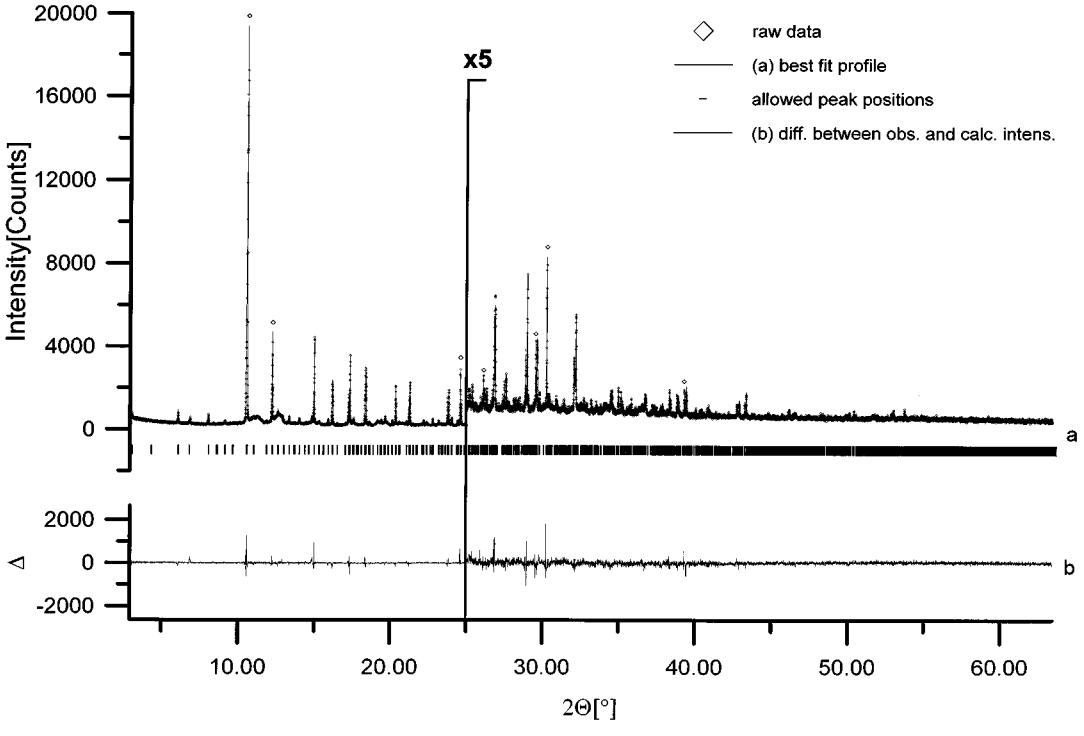

FIG. 5. The X-ray powder diffraction spectra of CAM in its tetragonal T1 phase at 604 K. Note that the peak at $2\theta = 6.9°$ does not fit in either of the tetragonal reciprocal lattices or the cubic reciprocal lattice. It is considered to be due to an impurity phase.

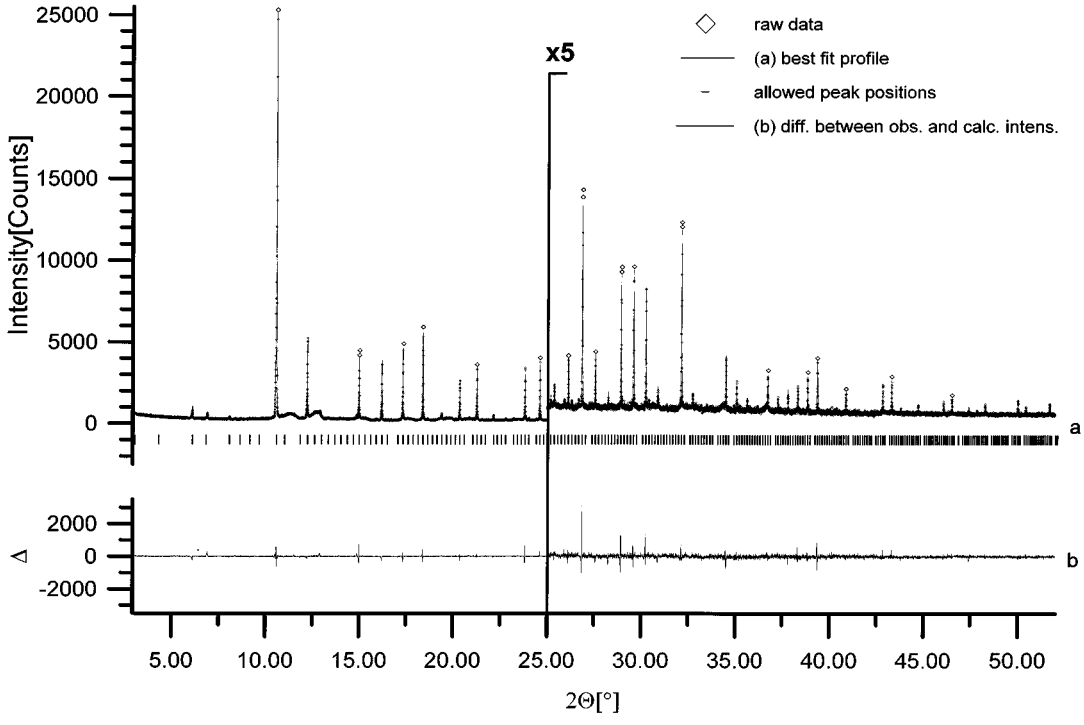

FIG. 6. The X-ray powder diffraction spectra of CAM in its tetragonal T2 phase at 614 K.

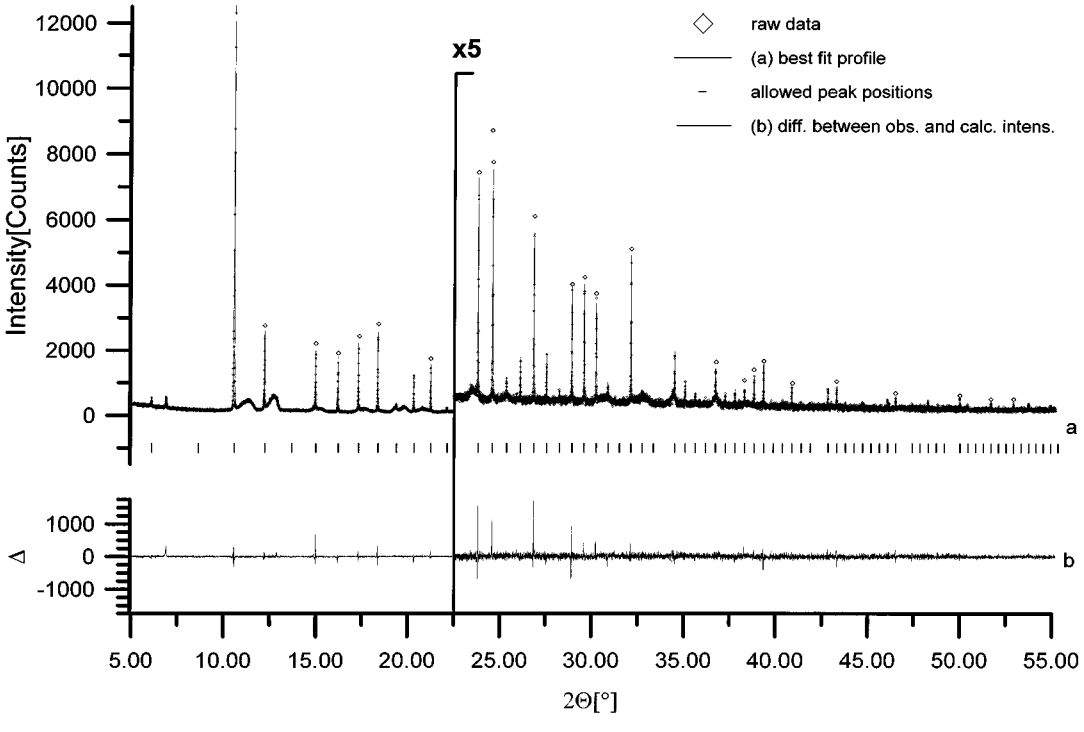

FIG. 7. The X-ray powder diffraction spectra of CAM in its cubic phase at 648.5 K.

TABLE 2
Coordinates from the Final Refinement of Orthorhombic CAM at 298 K

Atom	Occupation fraction	x	y	z	$100U_{iso}$
Ca1	1	0.01792 (13)	0.26458 (29)	0.2035 (5)	0.64 (6)
Ca2	1	0.25015 (21)	0.25932 (30)	0.2515 (5)	0.98 (6)
Ca3	1	− 0.13735 (12)	0.02258 (30)	0.2799 (5)	0.64 (6)
Ca4	1	− 0.12009 (12)	0.48644 (33)	0.2496 (5)	0.98 (6)
Al1	1	0.18476 (24)	− 0.1246 (4)	0.0073 (8)	0.55 (5)
Al2	1	0.43744 (23)	0.1167 (4)	− 0.0220 (6)	0.55 (5)
Al3	1	0.30978 (25)	0.1265 (4)	0.0103 (8)	0.55 (5)
Al4	1	0.44122 (23)	0.3674 (4)	− 0.0009 (7)	0.55 (5)
Al5	1	0.257254 (17)	0.0019 (4)	0.2601 (9)	0.40 (11)
Al6	1	0.0	0.0	0.2332 (10)	0.63 (12)
Al7	1	0.5	0.0	0.2442 (11)	0.63 (12)
O1	1	− 0.1248 (4)	0.4155 (8)	0.0166 (13)	0.04 (6)
O2	1	0.1202 (4)	0.3942 (8)	0.5490 (13)	0.04 (6)
O3	1	− 0.0194 (4)	0.1139 (8)	0.1390 (12)	0.04 (6)
O4	1	0.2947 (4)	0.1009 (9)	0.1803 (11)	0.04 (6)
O5	1	0.4668 (4)	0.0873 (8)	0.1402 (12)	0.04 (6)
O6	1	0.2175 (4)	− 0.0760 (8)	0.1480 (12)	0.04 (6)
O7	1	0.4542 (4)	0.2438 (8)	− 0.0630 (11)	0.04 (6)
O8	1	0.2934 (4)	0.2465 (8)	− 0.0209 (11)	0.04 (6)
O9	1	0.4525 (4)	− 0.0668 (8)	0.3350 (11)	0.04 (6)
O10	1	0.2855 (4)	0.5490 (8)	0.3720 (11)	0.04 (6)
O11	1	− 0.0529 (4)	− 0.0346 (7)	0.3221 (11)	0.04 (6)
O12	1	0.1937 (4)	0.4263 (8)	0.3221 (12)	0.04 (6)
O13	1	− 0.1044 (4)	0.3676 (9)	0.4137 (14)	2.22 (17)
O14	1	− 0.1670 (5)	0.1824 (10)	0.3726 (12)	2.22 (17)
O15	1	− 0.0889 (5)	0.1801 (9)	0.5852 (12)	2.22 (17)
O16	1	− 0.1776 (4)	0.3100 (10)	0.6279 (13)	2.22 (17)
Mo	1	0.13649 (5)	0.24003 (13)	0.0021 (4)	1.59 (3)

Note. Given are the position coordinates (x, y, z) with respect to the unit cell, and the temperature factors U_{iso} in Å^2. Symmetry applies as given in (19). Standard deviations are given in parentheses.

In both tetragonal phases we find highly irregular AlO_4 tetrahedra (Tables 7 and 8). The variation in the Al–O distances is larger in the tetragonal phases than in the cubic and in the orthorhombic phases. More importantly, the average of the four Al–O distances within one tetrahedron varies much more in the tetragonal phases than in the other two phases (Table 10). Whereas the average of the six O–Al–O angles within one tetrahedron is close to the ideal values of 109.5° for all atoms in all phases, the variation of the individual angles is again much larger in the tetragonal phase than in the other two phases (Table 10). These features show that the structure of the framework is less stable in the tetragonal phase than in the cubic and orthorhombic phases, and it thus explains the small existence region of the two tetragonal phases. The stability of the tetragonal phases then must come from a competition between stabilization through the entropy term, and stabilization by energetic terms. Both the disorder of the MoO_4^{2-} anions and the anion-framework bonding interaction in the tetragonal phase are in between the disorder and bonding in the orthorhombic and cubic phases.

4.2. Structural Variations at the Phase Transitions

In the previous section it was argued that the structure of the framework is less stable in both tetragonal phases than in the cubic and orthorhombic phases. Distortions of the framework then cannot be the driving force for the phase transitions. The structure determination of the cubic phase shows the MoO_4^{2-} tetrahedra to be highly disordered (Fig. 8). This is described by one oxygen atom (O2) giving rise to tetrahedra in six orientations, all of them considerably distorted. We think that no meaning should be attached to this refined position, other than that it is a convenient way to describe the continuous average electron density resulting from the disorder. The observed distortions are not to be given any meaning, and we must conclude that an accurate determination of the MoO_4^{2-} structures in the disordered phases is not possible from the Rietveld refinements.

Comparing the sizes of the cages with the sizes of the MoO_4^{2-} tetrahedra show the latter to have not only rotational disorder, but also disorder in the position of its center of mass (Mo atom). This is confirmed by the very high

TABLE 3
Coordinates from the Final Refinement of Tetragonal CAM (T1 Phase) at 604 K

Atom	Occupation fraction	x	y	z	$100U_{iso}$
Ca1	1	0.0276 (3)	0.2535 (5)	0.4691 (4)	3.10 (6)
Ca2	1	0.4911 (4)	0.2548 (5)	0.4940 (5)	3.10 (6)
Al1	1	0.3789 (5)	0.3789 (5)	0.75	0.86 (4)
Al2	1	0.1219 (5)	0.1219 (5)	0.75	0.86 (4)
Al3	1	0.1255 (5)	0.3716 (5)	0.7389 (8)	0.86 (4)
Al4	1	0.0	0.0	0.0	0.86 (4)
Al5	1	0.5	0.5	0.0	0.86 (4)
Al6	1	0.0	0.5	0.4882 (12)	0.86 (4)
Mo	1	0.26396 (12)	0.26396 (12)	0.250000	3.62 (6)
O1	1	0.5565 (10)	0.1027 (11)	0.4170 (18)	1.72 (10)
O2	1	− 0.0482 (11)	− 0.0980 (9)	− 0.0950 (18)	1.72 (10)
O3	1	− 0.0546 (12)	− 0.4060 (11)	− 0.1119 (16)	1.72 (10)
O4	1	− 0.4114 (12)	− 0.4140 (11)	− 0.4214 (13)	1.72 (10)
O5	1	0.5927 (6)	0.2499 (12)	0.2274 (15)	1.72 (10)
O6	1	0.9099 (7)	0.2363 (12)	0.2003 (13)	1.72 (10)
O7	0.5	− 0.2040 (14)	0.3468 (14)	0.6257 (24)	4.53 (40)
O8	0.5	− 0.2040 (14)	0.3468 (14)	0.8743 (24)	4.53 (40)
O9	0.5	0.1667 (18)	0.1874 (18)	0.1386 (24)	4.53 (40)
O10	0.5	0.3333 (18)	0.3126 (18)	0.3614 (24)	4.53 (40)

Note. Given are the position coordinates (x, y, z) with respect to the unit cell, and the temperature factors U_{iso} in Å^2. Symmetry applies as given in (19). Standard deviations are given in parentheses.

temperature factor as was obtained for Mo in the cubic phase (Table 5).

The refinement of the tetragonal T2 phase at $T = 614$ K shows that rotational disorder remains (Fig. 9). Disorder over two orientations now provides a sufficiently good description of the dffraction pattern. The reduced symmetry allows the Mo atom to shift along the line (x, x, 0.25), but it is found that the deviation from the cubic special position at

TABLE 4
Coordinates from the Final Refinement of Tetragonal CAM (T2 Phase) at 614 K

Atom	Occupation fraction	x	y	z	$100U_{iso}$
Ca1	1	0.0272 (7)	0.2494 (10)	0.4786 (11)	3.79 (7)
Ca2	1	0.4880 (7)	0.2491 (10)	0.4897 (12)	3.79 (7)
Al1	1	0.3779 (11)	0.3779 (11)	0.75	1.46 (5)
Al2	1	0.1263 (11)	0.1263 (11)	0.75	1.46 (5)
Al3	1	0.1282 (11)	0.3747 (11)	0.7410 (11)	1.46 (5)
Al4	1	0.0	0.0	0.0	1.46 (4)
Al5	1	0.5	0.5	0.0	1.46 (4)
Al6	1	0.0	0.5	0.4863 (18)	1.46 (4)
Mo	1	0.2546 (4)	0.2546 (4)	0.25	5.79 (8)
O1	1	0.5591 (22)	0.0984 (22)	0.4074 (31)	2.37 (15)
O2	1	− 0.0513 (22)	− 0.0923 (22)	− 0.1079 (38)	2.37 (15)
O3	1	− 0.0686 (22)	− 0.4132 (21)	− 0.0952 (33)	2.37 (15)
O4	1	− 0.3996 (22)	− 0.4237 (22)	− 0.4268 (30)	2.37 (15)
O5	1	0.5865 (18)	0.2485 (24)	0.1925 (25)	2.37 (15)
O6	1	0.9041 (19)	0.2596 (24)	0.2093 (27)	2.37 (15)
O7	0.5	− 0.1773 (23)	0.3323 (25)	0.6439 (19)	1.16 (38)
O8	0.5	− 0.1773 (23)	0.3323 (25)	0.8561 (19)	1.16 (38)
O9	0.5	0.2127 (16)	0.1550 (20)	0.1240 (32)	1.16 (38)
O10	0.5	0.2873 (16)	0.3450 (20)	0.3760 (32)	1.16 (38)

Note. Given are the position coordinates (x, y, z) with respect to the unit cell, and the temperature factors U_{iso} in Å^2. Symmetry applies as given in (19). Standard deviations are given in parentheses.

TABLE 5
Coordinates from the Final Refinement of Cubic CAM at 648.5 K

Atom	Occupation fraction	x	y	z	$100U_{iso}$
Al	1	0.25	0.5	0.0	2.19 (5)
O1	1	0.1571 (4)	x	0.4638 (6)	3.91 (13)
Ca	1	0.23155 (16)	x	x	4.80 (8)
Mo	1	0.0	0.0	0.0	6.27 (8)
O2	0.333	0.3676 (8)	x	0.4812 (32)	9.2 (9)

Note. Given are the position coordinates (x, y, z) with respect to the unit cell, and the temperature factors U_{iso} in Å^2. Symmetry applies as given in (19). Standard deviations are given in parentheses.

$x = 0.25$ is small (shift ≈ 0.09 Å). Some disorder of the position of Mo must remain, as its temperature factor remains large (Table 4). The refinement of the T1 phase at $T = 604$ K shows that it is related to a definite shift of Mo toward an off-center position within the cages (Fig. 10 and Table 3). The four MoO_4^{2-} tetrahedra are displaced toward the line $(0.5, 0.5, z)_t$ (shift ≈ 0.26 Å). The AlO_4 tetrahedra centered at $(0.5, 0.5, 0)_t$ and $(0.5, 0.5, 0.5)_t$ become fully expanded, albeit achieved through deformations rather than through rotation (see Section 4.1). (One out of four tetrahedra connecting the MoO_4^{2-}-containing cages is distorted in this way.)

The structure of the orthorhombic phase is fully ordered. The MoO_4^{2-} tetrahedra now are displaced along $\pm$ **a** (shift ≈ 0.33 Å), such that a "pairing" of tetrahedra occurs along **a**. The magnitude of the shift is slightly larger than in the T1 phase, whereby it should be realized that the orthorhombic phase has been determined at a temperature much lower than that at which the structures of the other three phases have been measured (Table 1). The gradual changes of the structures with temperature might then be responsible for this different magnitude. The major difference with the T1 phase is in the pattern of directions of the shifts (Figs. 10 and 11). The AlO_4 tetrahedra, connecting cages containing MoO_4^{2-} anions that have shifted toward each other, are almost in the fully expanded state, while the other half of the AlO_4 tetrahedra, now connecting cages containing MoO_4^{2-} anions that have separated, has a structure and orientation resembling the cubic phase (Fig. 11).

The orthorhombic and cubic phases of CAM are isostructural to the corresponding phases of CAW (4, 5). Instead of one tetragonal phase for CAW (6), we find two different tetragonal phases for CAM. An explanation for

TABLE 6
Interatomic Distances and Bonding Angles Characterizing the Tetrahedrally Coordinated Al Atoms for the Cubic Structure of CAM

Central atom	Coordinating atoms(s)	N_{sb}	Distance (Å) or angle (°)
Al	O1	4	1.729 (2) Å
Al	O1, O1	2	120.1 (4)°
Al	O1, O1	4	104.5 (2)°

Note. N_{sb} is the number of symmetry equivalent bonds or angles to occur within one tetrahedron about the central atom. Standard deviations are given in parentheses.

TABLE 7
Interatomic Distances and Bonding Angles Characterizing the Tetrahedrally Coordinated Al Atoms for the Tetragonal T2 Structure of CAM at $T = 614$ K

Central atom	Coordinating atoms(s)	N_{sb}	Distance (Å) or angle (°)
Al1	O4	2	1.77 (3) Å
Al1	O5	2	1.84 (3) Å
Al1	O4, O4	1	138.5 (21)°
Al1	O5, O5	1	123.5 (20)°
Al1	O4, O5	2	90.2 (12)°
Al1	O4, O5	2	109.4 (11)°
Al2	O2	2	1.71 (4) Å
Al2	O6	2	1.84 (3) Å
Al2	O2, O2	1	107.2 (22)°
Al2	O6, O6	1	117.2 (19)°
Al2	O2, O6	2	106.5 (13)°
Al2	O2, O6	2	109.6 (13)°
Al3	O1	1	1.68 (3) Å
Al3	O3	1	1.79 (3) Å
Al3	O5	1	1.77 (3) Å
Al3	O6	1	1.60 (3) Å
Al3	O1, O3	1	116.8 (16)°
Al3	O5, O6	1	125.0 (16)°
Al3	O1, O5	1	110.2 (16)°
Al3	O1, O6	1	106.1 (17)°
Al3	O3, O5	1	90.8 (14)°
Al3	O3, O6	1	108.0 (16)°
Al4	O2	4	1.71 (3) Å
Al4	O2, O2	2	110.0 (11)°
Al4	O2, O2	4	108.4 (21)°
Al5	O4	4	1.79 (3) Å
Al5	O4, O4	2	135.4 (17)°
Al5	O4, O4	4	98.3 (6)°
Al6	O1	2	1.80 (3) Å
Al6	O3	2	1.64 (3) Å
Al6	O1, O1	1	113.6 (20)°
Al6	O3, O3	1	125.0 (22)°
Al6	O1, O3	2	99.1 (11)°
Al6	O1, O3	2	110.3 (12)°

Note. N_{sb} is the number of symmetry equivalent bonds or angles to occur within one tetrahedron about the central atom. Standard deviations are given in parentheses.

TABLE 8
Interatomic Distances and Bonding Angles Characterizing the Tetrahedrally Coordinated Al Atoms for the Tetragonal T1 Structure of CAM at $T = 604$ K

Central atom	Coordinating atoms(s)	N_{sb}	Distance (Å) or angle (°)
Al1	O4	2	1.716 (3) Å
Al1	O5	2	1.745 (16) Å
Al1	O4, O4	1	137.1 (9)°
Al1	O5, O5	1	115.4 (8)°
Al1	O4, O5	2	95.4 (7)°
Al1	O4, O5	2	107.2 (7)°
Al2	O2	2	1.766 (16) Å
Al2	O6	2	1.626 (15) Å
Al2	O2, O2	1	118.3 (11)°
Al2	O6, O6	1	123.6 (9)°
Al2	O2, O6	2	103.1 (7)°
Al2	O2, O6	2	104.9 (6)°
Al3	O1	1	1.758 (17) Å
Al3	O3	1	1.733 (17) Å
Al3	O5	1	1.728 (17) Å
Al3	O6	1	1.870 (16) Å
Al3	O1, O3	1	115.6 (8)°
Al3	O5, O6	1	121.8 (6)°
Al3	O1, O5	1	99.5 (7)°
Al3	O1, O6	1	108.0 (7)°
Al3	O3, O5	1	106.9 (8)°
Al3	O3, O6	1	105.6 (7)°
Al4	O2	4	1.684 (14) Å
Al4	O2, O2	2	116.6 (10)°
Al4	O2, O2	4	106.1 (5)°
Al5	O4	4	1.778 (12) Å
Al5	O4, O4	2	131.3 (8)°
Al5	O4, O4	4	99.78 (29)°
Al6	O1	2	1.774 (16) Å
Al6	O3	2	1.704 (16) Å
Al6	O1, O1	1	120.2 (12)°
Al6	O3, O3	1	113.7 (11)°
Al6	O1, O3	2	104.8 (7)°
Al6	O1, O3	2	106.8 (6)°

Note. N_{sb} is the number of symmetry equivalent bonds or angles to occur within one tetrahedron about the central atom. Standard deviations are given in parentheses.

TABLE 9
Interatomic Distances and Bonding Angles Characterizing the Tetrahedrally Coordinated Atoms for the Orthorhombic Structure of CAM

Central atom	Coordinating atoms(s)	N_{sb}	Distance (Å) or angle (°)
Mo	O13	1	1.834 (13) Å
Mo	O14	1	1.766 (12) Å
Mo	O15	1	1.798 (11) Å
Mo	O16	1	1.719 (12) Å
Mo	O13, O14	1	109.9 (6)°
Mo	O13, O15	1	108.8 (5)°
Mo	O13, O16	1	107.5 (6)°
Mo	O14, O15	1	105.9 (6)°
Mo	O14, O16	1	113.6 (5)°
Mo	O15, O16	1	111.1 (6)°
Al1	O2	1	1.748 (11) Å
Al1	O6	1	1.689 (13) Å
Al1	O8	1	1.799 (12) Å
Al1	O12	1	1.863 (13) Å
Al1	O2, O8	1	118.0 (5)°
Al1	O6, O12	1	121.4 (6)°
Al1	O2, O6	1	105.3 (7)°
Al1	O2, O12	1	106.0 (6)°
Al1	O6, O8	1	107.8 (6)°
Al1	O8, O12	1	99.2 (6)°
Al2	O1	1	1.720 (11) Å
Al2	O5	1	1.737 (12) Å
Al2	O7	1	1.760 (11) Å
Al2	O11	1	1.823 (11) Å
Al2	O1, O7	1	120.8 (5)°
Al2	O5, O11	1	120.1 (5)°
Al2	O1, O5	1	100.5 (6)°
Al2	O1, O11	1	98.8 (6)°
Al2	O5, O7	1	106.7 (6)°
Al2	O7, O11	1	110.4 (6)°
Al3	O1	1	1.797 (11) Å
Al3	O4	1	1.666 (13) Å
Al3	O8	1	1.651 (12) Å
Al3	O10	1	1.757 (13) Å
Al3	O1, O8	1	122.9 (5)°
Al3	O4, O10	1	119.7 (6)°
Al3	O1, O4	1	97.6 (7)°
Al3	O1, O10	1	101.0 (6)°
Al3	O4, O8	1	107.3 (7)°
Al3	O8, O10	1	109.0 (7)°
Al4	O2	1	1.709 (11) Å
Al4	O3	1	1.679 (11) Å
Al4	O7	1	1.749 (11) Å
Al4	O9	1	1.779 (13) Å
Al4	O2, O7	1	117.5 (5)°
Al4	O3, O9	1	119.6 (5)°
Al4	O2, O3	1	109.7 (7)°
Al4	O3, O9	1	106.9 (6)°
Al4	O3, O7	1	105.8 (6)°
Al4	O7, O9	1	97.5 (6)°
Al5	O4	1	1.785 (12) Å
Al5	O6	1	1.790 (13) Å
Al5	O10	1	1.648 (12) Å
Al5	O12	1	1.720 (12) Å
Al5	O4, O6	1	119.2 (7)°

the occurrence of the three phases in CAW was the possibility of the XO_4^{2-} ion to bond to the framework in six orientations, which are equivalent for the cubic symmetry [9]. In the tetragonal phase only two orientations are selected, and the average position of the XO_4^{2-} ion may become off center. Here, we find a more complicated series of structures. In the orthorhombic phase the structure is fully ordered. The orthorhombic to T1 transition is related to the MoO_4^{2-} tetrahedra becoming orientationally disordered. The pattern of the shifts of these tetrahedra changes, whereby the magnitudes are almost equal in the two phases, but where the directions of the shifts of the different tetrahedra are

TABLE 9—*Continued*

Central atom	Coordinating atoms(s)	N_{sb}	Distance (Å) or angle (°)
Al5	O10, O12	1	120.6 (8)°
Al5	O4, O10	1	111.4 (6)°
Al5	O4, O12	1	98.5 (6)°
Al5	O6, O10	1	108.5 (5)°
Al5	O6, O12	1	107.6 (6)°
Al6	O3	2	1.800 (11) Å
Al6	O11	2	1.675 (10) Å
Al6	O3, O3	1	121.7 (9)°
Al6	O11, O11	1	120.7 (9)°
Al6	O3, O11	2	103.4 (5)°
Al6	O3, O11	2	104.5 (5)°
Al7	O5	2	1.731 (12) Å
Al7	O9	2	1.738 (11) Å
Al7	O5, O5	1	112.0 (10)°
Al7	O9, O9	1	121.7 (10)°
Al7	O5, O9	2	104.2 (5)°
Al7	O5, O9	2	107.5 (5)°

Note. N_{sb} is the number of symmetry equivalent bonds or angles to occur within one tetrahedron about the central atom. Standard deviations are given in parentheses.

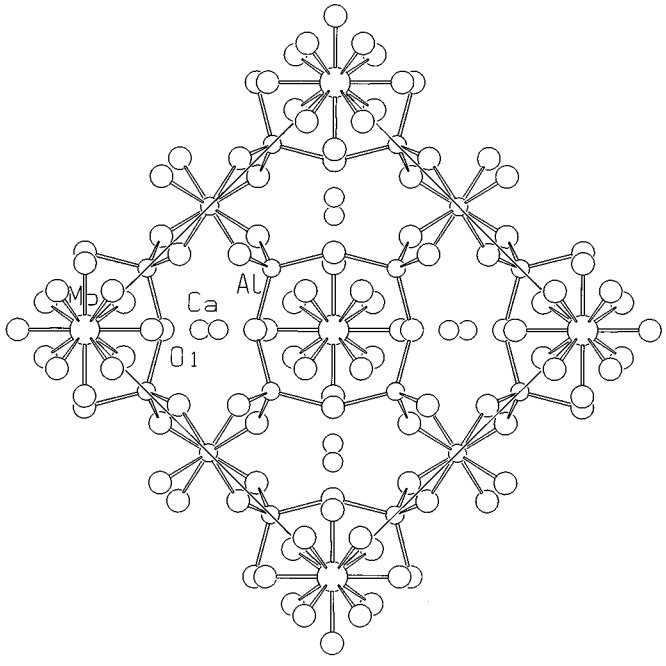

FIG. 8. Projection of the structure of the cubic phase of CAM along the cubic axis.

different. To achieve a transition from the one shift pattern to the other, the atoms must move over a distance of several times 0.1 Å, and it follows that the transition must be first order. The T1 to T2 transition is related to a release of the lattice strain, and microscopically, we find a change in the disorder of MoO_4^{2-} tetrahedra, while their shifts from the ideal positions is dramatically reduced. The T2 to cubic transitions then involves the MoO_4^{2-} tetrahedra becoming completely rotationally disordered. All phase transitions are accompanied by rather large distortions of the structure of the framework. We hope to obtain more detailed information about the disorder from an analysis of the observed diffuse scattering.

TABLE 10
Variations in the Framework Structure

	Orthorhombic	Tetragonal T1 at 604 K	Tetragonal T2 at 614 K	Cubic
d_{min}	1.65	1.63	1.60	1.73
d_{max}	1.86	1.87	1.84	1.73
d_{ave}	1.74	1.74	1.75	1.73
$\langle d\rangle_{min}$	1.73	1.68	1.71	1.73
$\langle d\rangle_{max}$	1.78	1.78	1.81	1.73
α_{min}	97.5	95.4	90.2	104.5
α_{max}	122.9	137.1	138.5	120.1
α_{ave}	109.8	109.7	109.7	109.7
$\langle\alpha\rangle_{min}$	109.5	109.5	108.9	109.7
$\langle\alpha\rangle_{max}$	111.0	110.3	110.7	109.7

Note. d represents an individual Al–O distance (in Å); $\langle d\rangle$ is the average value in one tetrahedron; and d_{ave} is the average value of all distances. α represents an individual O–Al–O angle (in °); $\langle\alpha\rangle$ is the average value in one tetrahedron; and α_{ave} is the average value of all angles.

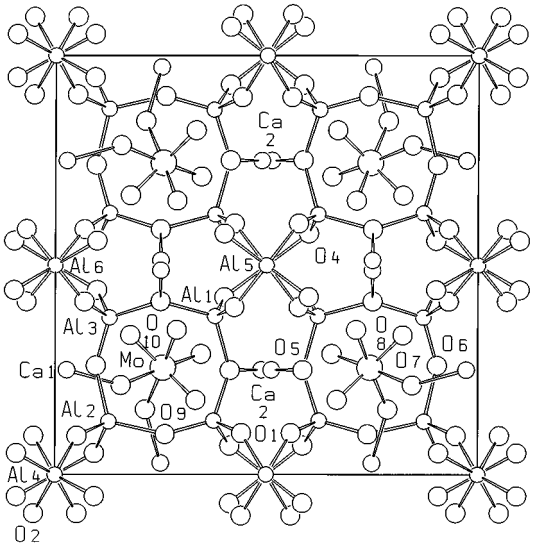

FIG. 9. Projection of the structure of the tetragonal T2 phase of CAM at 614 K along the short axis.

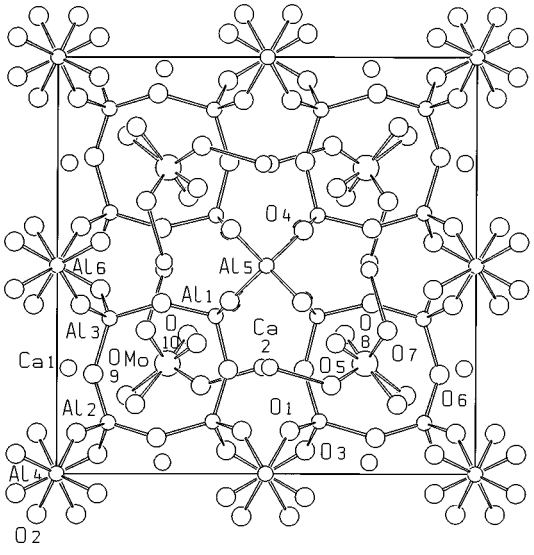

FIG. 10. Projection of the structure of the tetragonal T1 phase of CAM at 604 K along the short axis.

4.3. Nature of the Phase Transitions

In the present experiment, we have identified four phases above room temperature in CAM. Up to $T_{c1} \approx 590$ K the orthorhombic phase is stable; between T_{c1} and $T_{c2} \approx 604$ K the T1 tetragonal phase is stable; just above $T_{c3} \approx 612$ K we have found the T2 tetragonal phase; and above $T_{c4} \approx 624$ K the structure is cubic. Hysteresis of the transition from orthorhombic to T1 clearly shows this to be a first-order transition.

For the T2 to cubic transition it is noted that symmetry allows this to be a second-order transition, according to an irreducible representation at the reciprocal point $(\frac{1}{2}, \frac{1}{2}, 0)_c$. Furthermore, the temperature dependence of the intensity of the $(2, 1, 1)_t$ reflection in the region 614 to 624 K is in accordance with a second-order transition. Therefore, our results indicate that the cubic to T2 transition is of second order, with the transition temperature $T_{c4} \approx 624$ K. On further reducing the temperature below T_{c4}, the value of the order parameter increases, according to the increase of the intensity of the $(2, 1, 1)_t$ reflection (Fig. 2). The tetragonal phase is described by a $\sqrt{2}a \times \sqrt{2}a \times c$ supercell. In reciprocal space this is expressed by additional reflections at $(\frac{1}{2}, \frac{1}{2}, 0)$ from the cubic reflections. Then, the T2 phase can be described as a commensurate modulation of the cubic phase, with modulation wavevector $(\frac{1}{2}, \frac{1}{2}, 0)$.

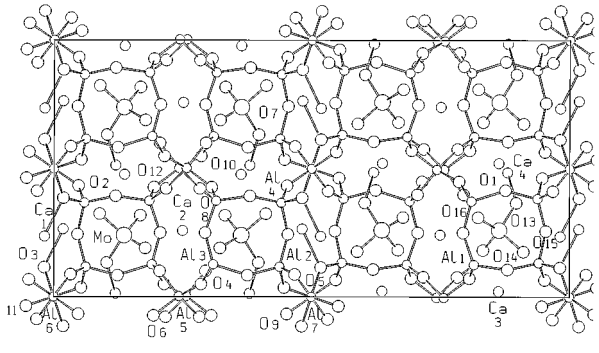

FIG. 11. Projection of the structure of the orthorhombic phase of CAM along the short axis.

The sudden development of spontaneous strain in the tetragonal lattice at T_{c3} proves the T2 to T1 transition to be first-order. Instead of one sharp transition, it is found that over a temperature interval of about 10 K both tetragonal phases coexist (Fig. 1). There is an onset of the transformation at T_{c3}, and the transformation is completed at T_{c2}. Both features are in accordance with the T2 to T1 transition being a martensitic transition (18), with the true transition temperature inbetween T_{c3} and T_{c2}. Alternatively it might be possible that the first-order transition is at T_{c3}. The gradual increase of the intensity of the $(2, 1, 1)_t$ reflection then should be interpreted as the development of order or further distortions of the framework on lowering the temperature, which then is completed at T_{c2}.

Our results are in accordance with preliminary experiments, which have shown that CAM should have two intermediate phases between orthorhombic and cubic (7). More recently, it was shown that differential scanning calorimetry (DSC) exhibits three anomalies during heating, at 603, 614, and 625 K, respectively (8). The correlation with our results is not entirely clear, as one martensitic transition with different temperatures for the onset and completion of the transformation, in itself should give rise to two anomalies in DSC (18). Then, one would expect four anomalies, at the four temperatures T_{c1} through T_{c4}, respectively. First, assuming the temperature readings in all experiments to be accurate within a few kelvin, the anomalies in DSC correspond with the onset of the T1 to T2 transition, the completion of this transition, and the T2 to cubic transition. The orthorhombic to T1 transition then was missed in the DSC experiment. Alternatively, assuming that either one of the experiments might have a systematic error in the temperature of about 10 K, the anomalies in the DSC can be related to the orthorhombic to T1 transition, and both the onset and completion of the T1 to T2 transition. The second-order transition at T_{c4} then would not have given rise to an anomaly in the DSC.

Electron diffraction in the T2 phase exhibited extra reflections, and it was concluded that the T2 is a modulated phase, although a modulation wavevector was not determined in (8). We failed to observe any (incommensurate) satellite reflections, other than the reflections corresponding to the tetragonal and orthorhombic supercell formations. Because

accurate temperatures and the indexings of the ED patterns are not available, a reinterpretation is difficult to make. One may speculate that it is actually the coexistence of the T1 and T2 phases which was interpreted as satellite reflections.

5. CONCLUSIONS

By synchrotron radiation X-ray powder diffraction we have identified four phases in CAM, as compared to only three phases in isostructural CAW. From the temperature dependence of the diffraction pattern, we have identified the highest temperature transition to be a second-order phase transition from a cubic structure toward a commensurately modulated structure with tetragonal supercell symmetry. The next transition was found to be a martensitic transformation with two "transition temperatures," corresponding to the onset and the completion of this phase transition. The lowest temperature transition is first order.

Refinements of the structures of all four phases allowed the microscopic origin of all transitions to be related to the change in the order/disorder of the cage anions MoO_4^{2-}. In the cubic phase the MoO_4^{2-} anions are disordered, both in their orientations and to some extent in their positions. At T_{c4} there is a change in the disorder, such that a superstructure develops, but with the cage anions on the average remaining approximately at the centers of the cages. The T2 to T1 transition is characterized by a displacement of the cage anions toward an off-center position within the cages, and this transition is accompanied with the sudden development of spontaneous strain in the lattice. At T_{c1}, the MoO_4^{2-} anions completely order, while the pattern of shifts out of the centers of the cages changes, such that the superstructure doubles and the symmetry reduces to orthorhombic.

ACKNOWLEDGMENTS

We are greatly indebted to D. Cox for making available the crystal heating device. P. Stephens is thanked for his continuous support. Research carried out in part at the National Synchrotron Light Source at Brookhaven National Laboratory, which is supported by the U.S. Department of Energy, Division of Materials Sciences and Division of Chemical Sciences. The SUNY X3 beamline at NSLS is supported by the Division of Basic Energy Sciences of the U.S. Department of Energy under Grant DE-FG02-86ER45231.

REFERENCES

1. D. Taylor, *Mineral. Mag.* **38,** 593 (1972).
2. P. Behrens, P. B. Kempa, S. Assmann, M. Wiebcke, and J. Felsche, *J. Solid State Chem.* **115,** 55 (1995).
3. L. Pauling, *Z. Kristallogr.* **74,** 213 (1930).
4. W. Depmeier, *Acta Crystallogr. Sect. B* **44,** 201 (1988).
5. W. Depmeier, *Acta Crystallogr. Sect. C* **40,** 226 (1984).
6. W. Depmeier, T. Vogt, and W. Buhrer, *Phase Transitions* **32,** 211 (1991).
7. W. Depmeier, *J. Alloys Compds.* **188,** 21 (1992).
8. L. Fischer, *Dipl. Thesis*, University of Keil, Germany, 1994.
9. W. Depmeier, *Phys. Chem. Miner.* **15,** 419 (1988).
10. P. Stephens, unpublished.
11. D. Cox, unpublished.
12. W. Depmeier, R. Melzer, and X. Hu, *Acta Crystallogr. Sect. B* **49,** 483 (1993).
13. R. Dinnebier, "GUFI," 1990.
14. R. B. von Dreele and A. C. Larson, Los Alamos National Laboratory Report LAUR 86-748, 1990. Updated version, May 1996.
15. P. Thomson, D. E. Cox, and J. B. Hastings, *J. Appl. Crystallogr.* **20,** 79 (1987).
16. L. W. Finger, D. E. Cox, and A. P. Jephcoat, *J. Appl. Crystallogr.* **27,** 892 (1994).
17. W. Depmeier, *Acta Crystallogr. Sect. B* **40,** 185 (1984).
18. F. E. Fujita, *in* "Physics of New Materials" (F. E. Fujita, Ed.), p. 139. Springer-Verlag, Berlin, 1994.
19. T. Hahn, (Ed.), "International Tables for Crystallography," Vol. A, fourth ed. Kluwer, Dordrecht, 1995.